VALIDATION OF GLOBAL AEROPROPULSIVE CHARACTERISTICS OF INTEGRATED CONFIGURATIONS

Frédéric Chalot[1]
Philippe Rostand[2]
Pierre Perrier[3]
Dassault Aviation, Saint-Cloud, France

Yurii P. Gounko[4]
Anatoly M. Kharitonov[5]
Albert F. Latypov[6]
Ignatii I. Mazhul[7]
Mikhail I. Yaroslavtsev[7]
ITAM, Novosibirsk, Russia

Abstract

An integrated scramjet experiment is proposed as an "Integration Validation Object." A model was tested in different facilities at ITAM with and without combustion. The behavior of the three-dimensional inlet was experimentally studied in great detail. As a first step in the validation process, we present the numerical reconstruction of the flow past the inlet at a Mach number of 6.

1. Introduction

In the course of the PREPHA program, a large scale effort has been initiated in France to develop the technologies and design methods required for the realization of an hypersonic airbreathing vehicle. The difficulties which must be overcome have been analyzed in numerous papers (see for example [1] and [2]). One of the key issues to consider is the very small performance margin of hypersonic airbreathing aircraft: the overall acceleration sums up to the difference of two contributors, the thrust and the drag, and can be orders of magnitude smaller than each of these two separate components. Accurate performance predictions are thus very difficult to perform.

The approach considered at Dassault Aviation to perform the design from an aerothermodynamic point of view is based on global CFD simulations which encompass the airframe and its propulsion system. In order to be included efficiently in the design process, these simulations must be carried out at reasonable cost and bear sufficient confidence in their level of accuracy. The latter can only be achieved through the careful validation of the global simulation tools.

The strategy retained to perform the global validation is based on the ground analysis of an integrated configuration, called an "Integration Validation Object" or IVO. Such an IVO must be representative of the integration problem of the real vehicle in flight (in terms of flow physics, fluid dynamics, and interaction between the different elements) and provide the conditions for the thorough evaluation of its performances in a ground facility. The comparison of theoretical and experimental predictions should validate the global CFD approach and enable the extrapolation to flight with *known* uncertainties.

Preliminary integration validation was performed using an existing axisymmetric experiment at ITAM. Results are described in [3]. This paper presents a new test case which was especially designed with the purpose of integration validation in mind and global thrust-minus-drag evaluation. The test case is defined in section 2. Section 3 is devoted to the presentation of the experimental set-ups in two different wind tunnels with and without combustion. Finally, the reconstitution of the inlet with a Navier-Stokes computation is described in section 4.

---

[1] Research Scientist, Member AIAA
[2] Head of Aerodynamic Modelization, Member AIAA
[3] Scientific Adviser, Member AIAA
[4] Head of Research Group
[5] Deputy Director
[6] Head of Laboratory
[7] Senior Scientist

2. Test case definition

The considered Integration Validation Object is the scramjet model with a three-dimensional inlet presented in Figure 1. The model consists of three parts: an inlet, a combustion chamber, and a nozzle which can be tested individually or in combination with each other. The investigated Mach numbers range from 4 to 8 and regimes with and without combustion should be compared.

The inlet is of side compression type. Its external compression is ensured by a horizontal ramp with a 12.5° slope and a straight leading edge, and two vertical wedges inclined by 10° and whose leading edges are swept by 45°. The inflection of the cowl lip and the internal contraction ratio were chosen according to the most severe starting condition ($M_\infty = 4$). The ratio of the throat area and of the inlet entrance area is 0.543. After the throat, the lower wall expands down with an angle of 2°. The inlet extends over a length of 400mm.

In order to isolate the inlet from the combustion chamber and avoid the influence of thermal choking over the inlet when testing the complete model with combustion, the duct section increases suddenly by 65% at the combustor entrance. Fuel is injected through 2 series of vertical struts. The combustion chamber is 315mm long. Starting at 155mm, the lower wall inclines down by 2°.

Finally a three-dimensional nozzle with a section ratio of 5.2 completes the model. It measures 145mm for a total length of the model of 860mm.

Tests can be conducted with the inlet alone, the inlet in conjunction with the combustion chamber, and with the full model. Although a few global results will be presented, we will focus in this paper on the detailed study of the inlet.

3. Experimental results

The experimental study of the thrust-minus-drag (total thrust-aerodynamic) characteristics of the scramjet model with three-dimensional inlet was conducted in wind tunnels of ITAM SB RAS. The inlet flow structure was studied in detail in the blowdown wind tunnel T-313 at Mach numbers $M = 4$ and 6, and the characteristics of the longitudinal force acting upon the model were measured on regimes without fuel supply. The thrust-aerodynamic characteristics were studied in the hot-shot wind tunnel IT-302 at Mach numbers $M = 6$ and 8 in a combustion mode, when gaseous hydrogen was supplied as a fuel, and on regimes without combustion. Similarity of the flow regimes in these wind tunnels related to the boundary layer state was ensured by using the boundary layer trips. This allowed one to compare the aerodynamic characteristics of the model, which were obtained for $M = 6$ in T-313 and IT-302.

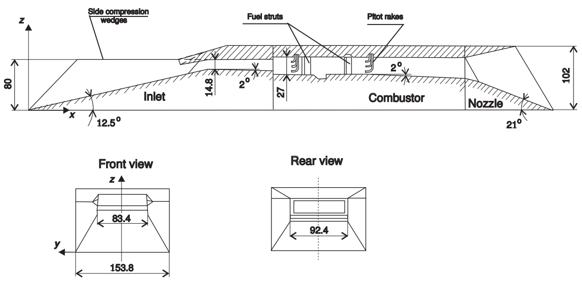

Figure 1. General view of the scramjet model (with section in the symmetry plane).

The model was mounted on vertical strut-pylons. The axial component of the resultant forces acting upon the model was measured by a specially designed external strain-gage balance installed on a strut under a shield. The system of fuel supply had a minor effect on the balance measurement. The model was also equipped with gages for the measurement of static pressure and heat flux distributions over the inlet ramp and engine duct, and also for the measurement of the Pitot pressure in two cross-sections of the combustion chamber (Figure 1).

3.1. Description of the facilities

As mentioned earlier, two different wind tunnels at ITAM SB RAS were used for this work: T-313 and IT-302M. Their respective characteristics are summarized below.

<u>T-313</u>

T-313 is a blowdown supersonic wind tunnel which covers the Mach number range 1.75–6. It can run in two different conditions: in the so-called “cold working contour,” the total temperature is close to the room temperature; in the “hot contour,” an electric heater can bring the total temperature up to 850K. The maximum total pressure reaches 16bar, which allows unit Reynolds numbers of 5 to 70 million. The duration of the run can extend to 10 minutes for the highest values of the total pressure; for lower total pressures, when the ejectors must be operated, this time is reduced to about 3 minutes. The testing chamber has a square section of 0.6×0.6m and is 2m in length. Finally, T-313 is equipped with a 4-component mechanical balance.

IT-302M

IT-302M is a hot-shot wind tunnel which is designed to accommodate Mach numbers from 5 to 18. The energy is supplied to the gas by an electric discharge in the plenum chamber at practically constant density. The maximum stagnation pressure if $p_0 = 100$bar and the maximum stagnation temperature $T_0 = 3000$K. The run duration is 0.05–0.15s. Different conical and contoured nozzles are available to cover the various Mach numbers; their exit diameters range from 200 to 300mm. The test section is an Eiffel chamber with a diameter of 800mm.

Two operation modes are available for this wind tunnel: the quasi-stable regime where total pressure and temperature drop in time, with a practically constant Mach number; and the regime where pressure is stabilized in the discharge plenum chamber using a two-step piston. The first mode can ensure higher pressure values in the plenum, and therefore higher Reynolds numbers. The maximum Reynolds number with respect to the nozzle exit diameter is 3–7 $\times 10^7$ for $M = 6$–8, and up to 2×10^8 for $M = 5$.

3.2. Isolated inlet experiments

Extensive isolated inlet experiments were carried out in T-313 at Mach numbers 4 and 6. A second inlet model was specially manufactured for this study: it was equipped with a large number of static pressure gauges (110 points over all the compression surfaces, and 21 points on the external surface of the cowl). Pitot pressure distribution was also measured at the inlet duct exit with a 5×5 probe rake. Schlieren visualization was permitted using removable optical silica glass side walls. This model is referred to as the "pressure-optical" model. Typical test conditions in T-313 are presented in the table below:

M_∞	4.04	5.89
P_0 (bar)	8.2–10.6	8.3
T_0 (K)	280–295	280–430
Re/m (10^6)	38.5–54	20–9.3

Three main test series were conducted in T-313 over the isolated inlet model. The first series was devoted to the checking of the inlet starting conditions at $M_\infty = 4$ and 6. The optical glass walls were mounted to allow for Schlieren visualization. Pressure measurements were only performed in the symmetry plane. In the two subsequent series, a more detailed study of the flow structure was conducted with the complete set of pressure taps; oil-film visualization of the streamlines was also used.

3.3. Combustion tests in IT-302M

The model tests with combustion were performed when the hot-shot tunnel operated with pressure stabilization in the settling chamber. At $M = 6$ the hydrogen was supplied in the regime with decreasing pressure in the fuel tank, the fuel-to-air ratio was $f = 0.7$–1.6. At $M = 8$ the pressure in the tank was kept constant and $f = 0.9$–1.4.

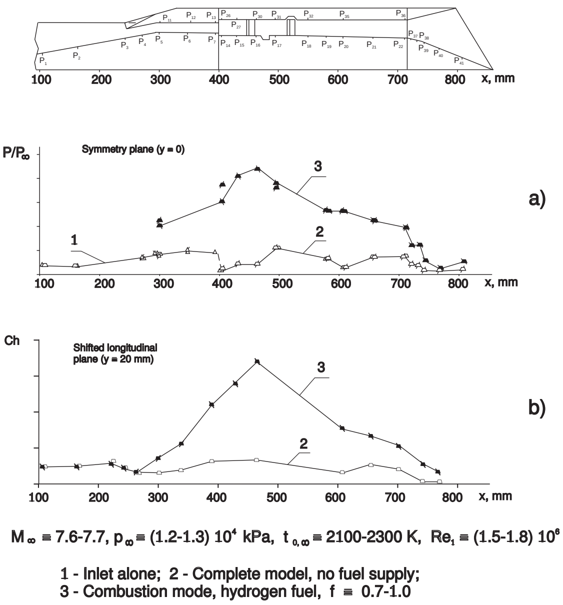

Figure 2. Lengthwise static pressure (a) and heat flux (b) distribution (lower wall).

Figure 2 shows the static pressure and heat flux distributions on the inlet ramp and on the lower wall of the engine duct for $M = 8$ and quasi-steady flow regime in the model within the time interval from 80 up to 120 ms. The data presented were obtained in model testing in the combustion mode and on the regime without fuel supply. The pressure is related to the free-stream pressure $p = p/p_\infty$, the heat flux is normalized by the flux of specific kinetic energy, $C_h = q_w/(\rho_\infty V_\infty V_\infty^2/2)$. Here p is the static pressure, ρ is the density, V is the flow velocity, q_w is the specific heat flux, the subscript ∞ refers to the free-stream parameters. The flow pattern in the engine duct was determined indirectly by the lengthwise pressure distribution in comparison with calculated one-dimensional estimates of flow characteristics with heat supply in the combustor. The reduced flow velocity estimates obtained on the basis of Pitot pressure measurement in the combustion chamber were taken into account. The level and character of the changes in pressure and heat fluxes along the engine duct show that both for $M = 8$ and $M = 6$ there were quasi-steady flow regimes in the engine duct with thermal choking, the flows with a pseudoshock realized in the inlet diffuser in these cases. In experiments without combustion a supersonic flow obtains in the inlet diffuser, and the levels of pressure and heat fluxes are respectively lower, Figure 2.

3.4. Force measurements

A key ingredient of the integration validation is to have access to individual force measurements over the different elements of the model, and the net drag of the elements interacting with each other. Particular care was thus taken in designing a reliable balance system.

<u>Balance design</u>

T-313 is equipped with a four-component (drag, lift, pitching and rolling moments) mechanical balance. In order to have access to force measurements in IT-302M for the higher Mach number tests with and without combustion, a special strain gage balance was developed. It measures the x and z components of the force and the pitching momemt; the normal force and the pitching moment are only used to correct for their influence on the longitudinal force measurement. An essential feature is that the balance woks under the conditions of dynamic loading in the hot-shot wind tunnel. It must be noted that redundant longitudinal force measurements were realized in T-313 using both the mechanical and the strain-gage balances.

<u>Balance measurements of the full model</u>

The results of balance measurements are presented in Figure 3 as the longitudinal force coefficient $C_x = F_x/(q_\infty A_0)$ versus the Mach number. Here F_x is the axial component of resultant force acting upon the model, $A_0 = 0.0123$ m^2 is the reference area (frontal area of the inlet), q_∞ is the dynamic pressure. The force measurement in T-313 was performed simultaneously by the mechanical balance, these data are shown in Figure 3.

The drag values obtained in IT-302 tests without fuel supply are everywhere slightly higher than the data obtained in T-313. This is explained by the difference in flow parameters, mainly, different Reynolds numbers in the tests in two wind tunnels. Thus, the Mach and unit Reynolds numbers were $M = 5.85$–6.0, $Re_1 \approx 2 \times 10^7$ 1/m in T-313 and $M = 5.6$–5.8, $Re_1 \approx 2 \times 10^6$ 1/m in T-302M. The model drag coefficient in the combustion mode decreases due to internal thrust by 0.32 for $M = 6$ and 0.35 for $M = 8$.

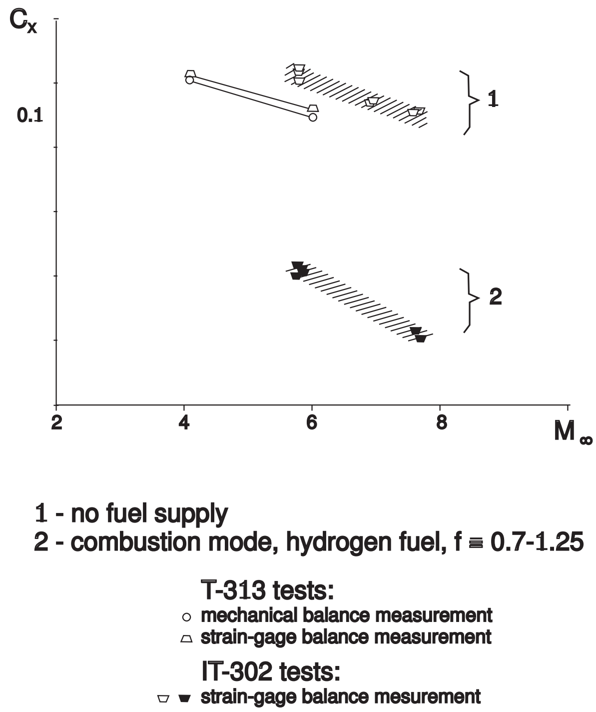

Figure 3. Coefficient of the total axial aerodynamic-thrust force for the complete model versus free-stream Mach number.

4. <u>Numerical reconstruction of the isolated inlet</u>

One of the requirement of the global CFD simulation is to be cost effective in order to be integrated in the design cycle. The general strategy would be to use an Euler + boundary-layer approach (see [3] and [4]). The heat addition in the combustor due to fuel injection is modeled using a 0-D transfer function provided by the engine designer.

A view of the full model surface is shown in Figure 4, where the inside duct can be seen through the mesh; the “hole” is where the 0-D model is active and couples the inlet with the nozzle.

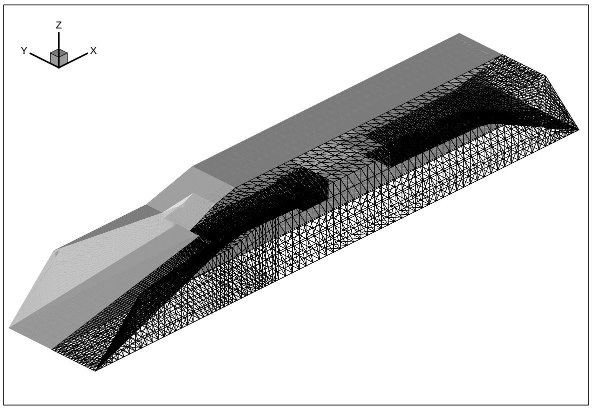

Figure 4. View of the complete model with the inside duct.

In order to evaluate the uncertainties of this method a detailed Navier-Stokes computation is performed over the isolated inlet. It will enable to assess the validity of the Euler + boundary-layer approach in the presence of shock reflections in the duct. It will provide a precise description of the flow distorsions in the inlet exit and give access to the actual mass flow rate through the inlet. Possible possible upstream effect of the high pressure levels generated by combustion, through the boundary-layers, could also be studied.

The Navier-Stokes mesh is presented in Figures 5 and 6. It was designed to compute the conditions of T-313 at a Mach number of 6: $p_0 = 8.2$bar and $T_0 =$ 280K. In order to capture the boundary-layer features the first grid points are located 10μm away from the model surface; this corresponds to a y^+ of the order of unity. The total mesh amounts to 784,830 nodes. It was split into 16 blocs for parallel processing.

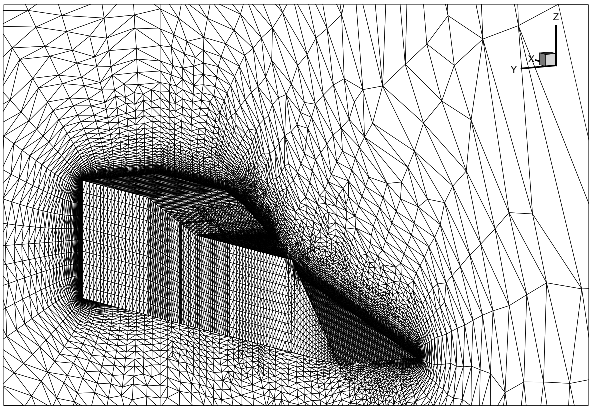

Figure 5. View of the surface mesh of the isolated inlet model.

Figure 6 shows an additional diverging section at the exit of the inlet. It is meant to make sure that the flow would be supersonic in the exit plane and would not cause problems during the inlet starting.

The computation was performed on an IBM SP2 using Dassault-Aviation's Navier-Stokes code called `VIRGINIE`. It uses a finite element approach, based on a symmetric form of the equations written in terms of entropy variables. The advantages of this change of variables are detailed in [5, 6, 7]. The stabilized finite element method, used in `VIRGINIE`, is called the Galerkin/least-squares formulation. It ensures good stability characteristics while retaining a high level of accuracy. The local control of the solution in the vicinity of sharp gradients is further enhanced by the use of a nonlinear discontinuity-capturing operator. Convergence to steady state is achieved through a 1st-order fully implicit iterative time-marching procedure based on the GMRES algorithm (see [8]). The presented computation was performed using a two-layer k–ε model, whose equations are solved in a staggered manner and coupled with the Navier-stokes equations through the turbulent viscosity.

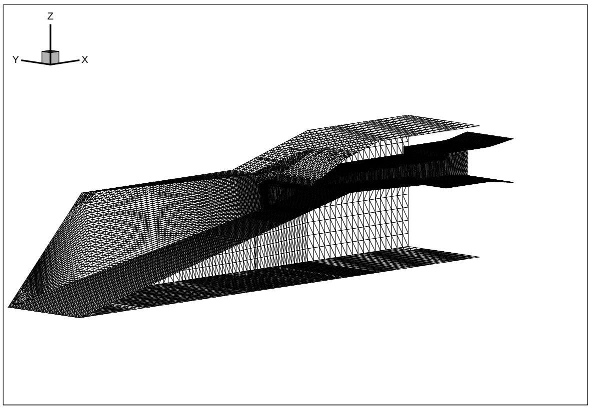

Figure 6. Surface mesh of the isolated inlet model viewed from the symmetry plane.

Figures 7 and 8 show the Mach number contours, respectively around the inlet and in the symmetry plane (half the model was computed). The three-dimensional interaction of the shocks induced by the compression ramps and the cowl can be seen in Figure 7. The thickness of the boundary layer entering the inlet at the cowl level is quite important (Figure 8). The thickening of the boundary-layer is due to two factors: first, the interaction with the shocks coming from the side compression wall generates high turbulence levels; the fixed wall temperature boundary conditions ($T_{\text{wall}} = 280$K) tends to lower the effective Reynolds number close to the wall due to the important heat transfer.

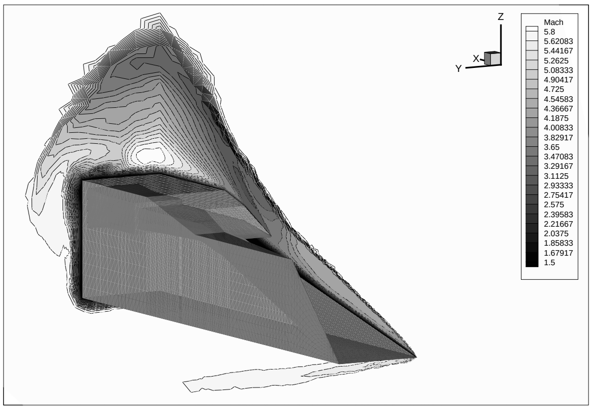

Figure 7. Mach number contours over the inlet ($M_\infty = 6$, T-313 conditions).

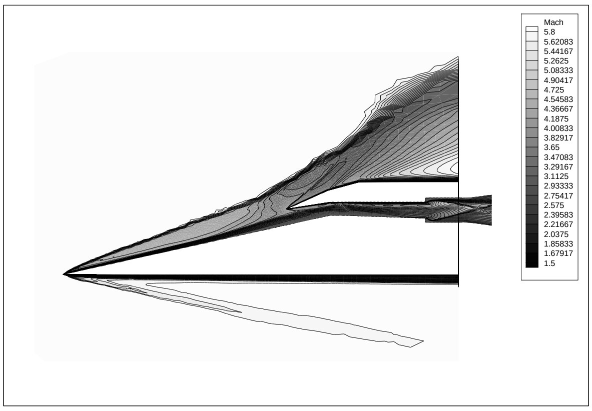

Figure 8. Iso-Mach lines in the symmetry plane ($M_\infty = 6$, T-313 conditions).

The pressure contours in the plane of symmetry presented in Figure 9 show the system of shock reflections in the inlet duct. The shock induced by the cowl lip seems to impinge the lower surface as a normal shock, which is not observed in the Schlieren pictures of the same region. In fact the flow structure appears extremely three-dimensional in this region as can be seen in Figure 10. The shock interaction in the symmetry plane and along the outside wall are quite different. Moreover, the pressure increase over the horizontal ramp seems to occur gradually in compression waves rather than suddenly in sharp shocks. Due to the interaction with the turbulent boundary layer the oblique shocks which emanate from the wedges leading edges progressively transform into fans of compression waves. Theses waves, rather than defined shicks, intersect in the symmetry plane forming the observed pressure distribution.

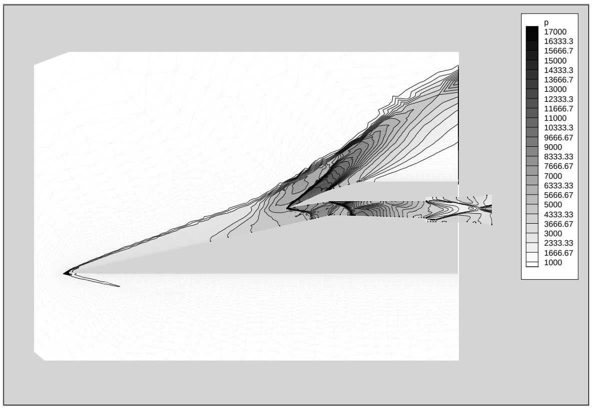

Figure 9. Iso-pressure lines in the symmetry plane ($M_\infty = 6$, T-313 conditions).

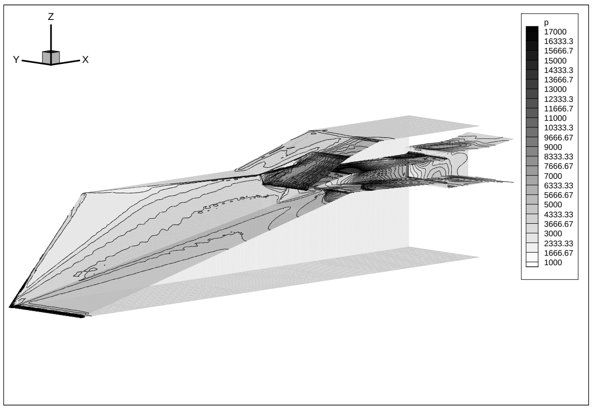

Figure 10. Iso-pressure lines over the surface of the inlet ($M_\infty = 6$, T-313 conditions).

The slow rise in pressure distribution can be seen clearly in Figure 11, which compares the values measured in the symmetry plane during the three test series at T-313 with the present calculation. However the computed level of pressure in front of the inlet entrance appears higher than that observed during the experiments. Although every effort was made to ensure rapid transition to a fully turbulent boundary-layer with tripping devices places as close as possible to the compression ramp leading edges, the interaction may still be transitional in the experiment. Two pressure levels are indicated in Figure 11: they correspond respectively to a three-dimensional laminar and turbulent boundary-layer separation. Although the experimental pressure profile goes through the laminar level without reaching the turbulent one, the computed pressure gradually rise to reach the theoretical turbulent separation level in front of the entrance of the inlet inside duct. Since the computation is clearly turbulent from the start, this might be an indication that the flow (at least in the symmetry plane) does not transition to full turbulence until the cowl region. This, of course, must be further investigated; comparison with a laminar computation would definitely help understanding the phenomenon.

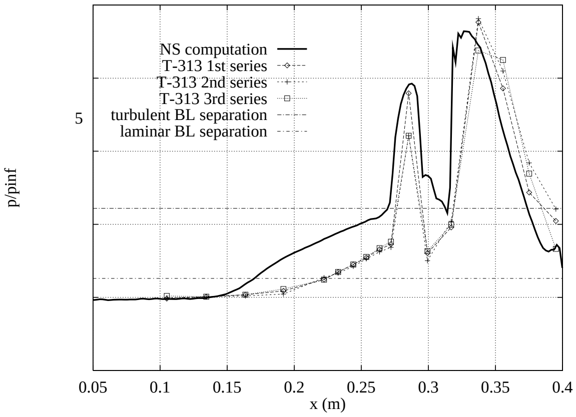

Figure 11. Comparison of the computed longitudinal pressure distribution with the measures of the three test series in T-313.

Figure 12 shows the comparison between the pressures measured in the B-B section, located at $x = 299.3$mm from the inlet leading edge, with the Navier-Stokes result. This section corresponds to the throat region. Both the experiment and the computation show little variation along the lower surface and the side wall located at $y = 41.7$mm. However, the pressure level increases abruptly along the internal surface of the cowl. The final levels obtained experimentally and numerically differ somewhat on the first half of the top wall (close to the symmetry plane).

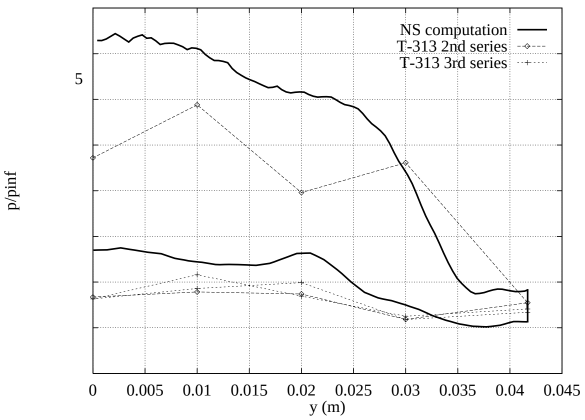

Figure 12. Comparison of the computed pressure distribution in the B-B plane ($x = 299.3$mm) with the measures of the 2nd and 3rd test series in T-313.

5. Conclusion

An new integrated scramjet experiment is proposed as an "Integration Validation Object." A model was tested in different wind tunnels at ITAM with and without combustion. Rich experimental data are available. So far only measurements concerning the isolated inlet at Mach 6 have been compared to a three-dimensional turbulent Navier-Stokes computation. The validation must be carried on to the full integrated simulation.

Acknowledgements

The work presented here has been partially funded by DGA, CNES, and MRT in the framework of the PREPHA program. The collaboration with ITAM is funded by DRET in the framework of Franco-Russian cooperations.

The authors are particularly grateful towards a number of Dassault-Aviation staff members for their help in realizing the computations presented here: D. Alleau, J.P. Figeac, J.M. Hasholder, S. Kleinveld, and M. Ravachol.

References

[1] P. Perrier, Ph. Rostand, and B. Stoufflet, "Integration of an air-breathing hypersonic airplane," paper #93-5032, *AIAA 5th NASP Conference*, München, Germany, 1993.

[2] P. Perrier and Ph. Rostand, "Hypersonic airbreathing aircraft integration through CFD: global simulations for global thinking," paper #94-3090, *30th Joint AIAA/SAE/ASME/ASEE Propulsion Conference and Exhibit*, Indianapolis, 1994.

[3] P. Perrier, B. Stoufflet, Ph. Rostand, V.K. Beav, A.F. Latypov, V.V. Shumsky, and M.I. Yaroslavtsev, "Integration of an hypersonic airbreathing vehicle: assessment of overall aerodynamic performances and of uncertainties," paper #95-6100, *AIAA 6th International Aerospace Planes and Hypersonics Technologies Conference*, Chattanooga, TN, April 3–7, 1995.

[4] M.P. Leclercq, B. Mantel, J. Périaux, P. Perrier, and B. Stoufflet, "One recent 3-D Euler computations around a complete aircraft using adaptive unstructured mesh refinements," *2nd World Congress on Computational Mechanics*, Stuttgart, Germany, August 27–31, 1990.

[5] F. Chalot, T.J.R. Hughes, and F. Shakib, "Symmetrization of conservation laws with entropy for high-temperature hypersonic computations," *Computing Systems in Engineering*, Vol. 1, pp 495–521, 1990.

[6] F. Chalot and T.J.R. Hughes, "A consistent equilibrium chemistry algorithm for hypersonic flows," *Computer Methods in Applied Mechanics and Engineering*, Vol. 112, pp 25–40, 1994.

[7] F. Chalot, M. Mallet, and M. Ravachol, "A comprehensive finite element Navier-Stokes solver for low- and high-speed aircraft design," paper #94-0814, *AIAA 32nd Aerospace Sciences Meeting*, Reno, NV, January 10–13, 1994.

[8] F. Chalot, Q.V. Dinh, M. Mallet, A. Naïm, and M. Ravachol, "A multi-platform shared- or distributed-memory Navier-Stokes code," *Parallel CFD '97*, Manchester, UK, May 19–21, 1997.